Technische Universität München
Fakultät für Physik

Abschlussarbeit im Bachelorstudiengang Physik

Baryonic feedback and small-scale problems in hydrodynamical ΛCDM simulations

Leonard Romano

4. Februar 2019

Osaka University Theoretical Astrophysics Group

Erstgutachter (Themensteller): Prof. B. Garbrecht

Contents

Abstract

This thesis is part of a larger study, in which the effects of baryonic feedback and star formation on hydrodynamical simulations of isolated galaxies and zoom-in galactic simulations in the ΛCDM framework are being studied and analysed in relation to small-scale problems. Here I analyse the rotation curves, dark matter(DM) radial density profiles and DM velocity distributions of simulations, which are part of the *AGORA* project [1, 2], run by members of the Osaka University theoretical astrophysics group. My results for isolated galaxy simulations show that the snapshot at $t \approx 1\,\mathrm{Gyr}$ resembles the Milky Way(MW) the most, and I also give hints at how to improve the initial conditions for further studies. Furthermore I present the results of the analysis of several milky-way-like galaxies in galactic scale simulations, which show that baryonic feedback can in fact reproduce a cored DM density profile. I also calculate the local DM mass density for each snapshot and find that the values are within a factor of 1,5 to the observed value $\rho_\odot = (0{,}30 \pm 0{,}03)\,\mathrm{GeV\,cm^{-3}}$ [3].

Chapter 1

Motivation: Cosmological Simulations

In the early 1930s observations of galaxy clusters revealed that a large amount of unobserved matter was needed to explain the observed data [4]. This lead to the hypothesis of DM a type of matter that only interacts by gravity and does not emit any light. Soon a cosmological amount of theories began to rise trying to explain the nature of this DM. Out of this cluster of theories one theory called ΛCDM, which is nowadays sometimes also referred to as "standard model of cosmology"[5], emerged combining Dark Energy (Λ) with cold collisionless dark matter (CDM). ΛCDM has been very successful describing the large scale structure of the universe and structure formation in scales of order $\mathcal{O}(Mpc)$ [6]. This is also strongly supported by a large number of simulations. However on smaller scales ΛCDM seems to fall apart. Since the 1990s four main differences between theory and observation came to light [6, 7]:

- *Cusp-core problem*: Many high resolution numerical ΛCDM simulations reproduce very cuspy profiles that asymptotically scale as $\rho_{DM} \propto r^{-1}$[8, 9, 10] in the inner region. Yet a great number of observed DM density profiles depict a cored profile that scales as $\rho_{DM} \propto r^{0}$[11, 12, 13] for small radii. This discrepancy is known as cusp-core problem[6, 7].

- *Diversity Problem*: Cosmological structure formation is predicted to be a self-similar process with hardly any scatter in density profiles for halos of given mass[10, 14]. However a much larger scatter in their interior [15] and variations of inferred core densities up to factors of $\mathcal{O}(10)$ [16] have been observed for disk galaxies with the same maximal circular velocity.

- *Missing satellites problem*: CDM halos are predicted to have a large abundance of substructure, as they grow via hierarchical mergers of smaller halos surviving them [17]. However, the observed number of small galaxies in the Local Group field is fewer than predicted by the simulations. In the MW, simulations predict an abundance of $\mathcal{O}(100 - 1000)$ for subhalos that can host galaxies, yet at the time this problem was raised only 10 dwarf spheroidal galaxies had been found [18, 19]. Field galaxies in close proximity to the MW are depicting a similar underabundance of missing substructure compared to the velocity function

predicted by simulations [20, 21, 22]. However new observational results suggest that this problem might have just been resolved with a large number of substructure observations being made [23].

- *Too-big-to-fail problem*(TBTF): In the past few years, the most luminous satellites in the MW were subject to a great number of studies as they are expected to be host to the most massive subhalos in ΛCDM simulations. However, the central densities of these subhalos have been shown to be inconsistent with the stellar dynamics of the brightest dwarf spheroidals [24, 25]. The name "Too-big-to-fail" arises from the expectation that subhalos that are so massive are too big to fail forming stars and should therefore host observable galaxies. Studies of dwarf galaxies in Andromeda [26] and the Local Group field [27] have found similar issues.

To resolve these problems a great number of numerical simulations has been run, employing all kinds of theories, including self-interacting dark matter(SIDM)[6], weakly-interacting massive particles (WIMPs)[28, 29], Modified Newtonian Dynamics (MOND)[30, 31, 32], negative mass particles [33] and for this thesis most notably baryonic feedback [7, 6]. Among these baryonic feedback is one of the most popular theories, probably being the the hope of the ΛCDM paradigm as it does not require ΛCDM to be overthrown.
The *AGORA* project is a "comprehensive numerical study of well-resolved galaxies in the ΛCDM cosmology"[1]. Its aim is to make the different simulation codes, that have evolved independent of one another over time, comparable as to guarantee that different results in simulations are just due to different physics employed and not due to different numerical methods applied.

Chapter 2

Simulation Code

In this chapter I will introduce the simulation code used to produce the data analysed in this thesis. The code is mostly described in the original *AGORA* paper [1], but I will shortly revise all the important facts in the following.

2.1 Overview

The simulations analysed in this thesis were run by members of the Osaka University Theoretical Astrophysics Group (OUTAP) using GADGET-3 which is a upgraded version of the N-Body+SPH code GADGET-2 developed by Volker Springel [34, 35][1] and which has been used for *Aquarius* one of the highest resolution zoom-in collisionless simulations [36].
The code maps the three dimensional domain on a one dimensional line using a Peano-Hilbert Curve and then splits this line in fragments which are then used for calculations on different processors. This method makes sure that the interparticle forces are up to round-off errors not depending on the number of processors. Gravity is calculated using a tree approach, that assigns the particles to "nodes" and then uses a multipole expansion to approximate the node-particle forces. The time integration happens using a kick-drift-kick leapfrog integrator that is fully symplectic for constant timesteps for all particles. The simulation is sped up using individual and adaptive timesteps, which are based on a power-of-two subdivision of the long-range timestep.

2.2 Initial Conditions

There are different initial conditions implemented for the isolated galaxy simulation and the zoom in simulation.

[1] The simulation code is available at:
https://wwwmpa.mpa-garching.mpg.de/gadget/

2.2.1 Isolated Galaxy Initial Conditions

The isolated galaxy is initialised using the MakeDisk code written by Volker Springel. It solves the Jeans equations for a "quasi-equilibrium multi-component halo/disk/bulge collisionless system"[1] with thermal equilibrium velocity distributions for all particles. The dark matter halos density has a so called NFW profile (Navarro–Frenk–White)[10]:

$$\rho_{NFW} = \frac{4\rho_s}{\frac{r}{r_s}\left(1+\frac{r}{r_s}\right)^2} \tag{2.1}$$

Where $r_s = R_{vir}/c$ with the concentration parameter c, the virial radius R_{vir} and $\rho_s = \rho_{crit}\frac{\Delta_{vir}\Omega_m}{12}\frac{c^3}{f(c)}$, where $f(c) = \log(1+c) + \frac{c}{1+c}$. Here $\rho_{crit} = \frac{3H^2}{8\pi G}$ is the present time critical density of the universe, Δ_{vir} is the overdensity parameter and Ω_m is the mass density parameter. The NFW profile is completely determined by the halo mass $M_{200} = 1{,}074 \times 10^{12}\mathrm{M}_\odot$ and concentration parameter $c = 10$. Furthermore the spin parameter $\lambda = 0.04$ and $v_{c,200} = 150\,\mathrm{km\,s^{-1}}$ which results in a virial radius $r_{200} = 205{,}4\,\mathrm{kpc}$. The disk is distributed with an exponential profile (in cylindrical radius r and height z) of scale length $r_d = 3{,}432\,\mathrm{kpc}$ and scale height $z_d = 0.1\,r_d$. It is decomposed in a stellar component of $M_d = 4{,}297 \times 10^10\mathrm{M}_\odot$ and a gas disk with a gas fraction of $f_{gas} = \frac{M_{gas}}{M_d} = 0.2$. Lastly there is a stellar bulge following the Hernquist profile [37] with a bulge-to-disk mass ratio of $B/D = 0.1$. We were running the a slightly higher resolution version of the low resolution simulation with $N_{DM} = 3 \times 10^5$, $N_d = 3 \times 10^5$, $N_B = 3.75 \times 10^4$ and $N_gas = 3 \times 10^5$. The initial disk Temperature is $T = 10^4\,\mathrm{K}$.

2.2.2 Cosmological Initial Conditions

The initial conditions for the zoom-in simulation are implemented using the Music code (MUlti-Scale Initial Conditions)[38][2], which uses real space convolution with an adaptive multi-grid Poisson solver to initialise the density, particle displacement and velocity fields with high accuracy suitable for multi-scale zoom-in structure formation simulations.
Density perturbations for the baryon and the CDM fluid are assumed to be equal, following the total matter density perturbations. To minimise two-body effects the "baryon particles are generated on a staggered lattice with respect to the CDM particles and displaced by the same displacement field as the CDM particles evaluated at the staggered positions"[1]. The temperature is initially set to the mean baryonic temperature at the starting redshift.

[2]The IC-code is available at:
http://bitbucket.org/ohahn/music/

The code generates the fields on a range of nested levels n of effective linear resolution 2^n. The level covering the entire domain is called n_{min}, the maximum level n_{max}. In this thesis I am analysing snaps of simulations run at $n_{max} = 10$ and $n_{max} = 11$. The entire simulation is then defined entirely by a string of numbers which is used as a seed to create random noise fields. This allows for high resolution regions to be shifted or enlarged without breaking consistency. For the merger history a quiescent merger history with a small number of mergers between redshifts $z = 2$ and $z = 0$ was chosen. The ΛCDM parameters used are consistent with the *Planck* 2015 results [39] based on observations of temperature and polarisation anisotropies of the CMB combined with Planck temperature and lensing data as well as Planck LFI polarisation measurements: $\Omega_m = 0.3089$, $\Omega_\Lambda = 0.6911$, $\sigma_8 = 0.815$, $n_s = 0.968$ and $H_0 = 67{,}74\,\mathrm{km\,s^{-1}\,Mpc^{-1}}$. We are assuming that radiation energy and curvature are negligible: $\Omega_R = \Omega_k = 0$. The high resolution region in the centre was set to have a size $V \sim (5 \times 5 \times 5)$ $\mathrm{cMpc^3h^{-3}}$ nested inside of a $V_{box} = (50 \times 50 \times 50)$ $\mathrm{cMpc^3h^{-3}}$ box.

2.3 Physics Package

The physics employed include metallicity-dependent gas cooling, UV background, stellar IMF, star formation, metal and energy yields by SNe, and stellar mass loss. They are crucial for the outcome of the simulation, which is why I am going to explain them in the following.
Chemistry and gas cooling is handled by the library Grackle [40][3] which provides a non equilibrium primordial chemistry network for H and He, Compton cooling off the cosmic microwave background(CMB), tabulated metal cooling and photo-heating rates, which are calculated using the code Cloudy [41][4]. The exact method of gas cooling is explained in the original *AGORA* paper [1].
Star formation obeys the following law:

$$\frac{d\rho_\star}{dt} = \frac{\epsilon \rho_{gas}}{t_{ff}} \tag{2.2}$$

where $\rho_\star$ and ρ_{gas} are the stellar and gas density, respectively, ϵ is the star formation efficiency and $t_{ff} = \sqrt{3\pi / (32 G \rho_{gas})}$ is the local free-fall time. Furthermore, below a certain density threshold star formation is forbidden and a non-thermal pressure floor is applied to prevent grid cells from collapsing gravitationally, avoid artificial fragmentation and stabilise scales of order the smoothing length. The star formation

[3] Grackle is available at:
http://grackle.readthedocs.org/
[4] Cloudy is available at:
http://www.nublado.org/

density threshold, the star formation efficiency, the initial mass of star particles and the stochasticity of star formation were tuned using previous simulations.
The UVB is implemented using the models by Haardt & Madau [42].
Each star particles represents a simple stellar population with age, metallicity and a initial mass function (IMF) as proposed by Chabrier [43]:

$$\frac{dn}{dm} \propto \begin{cases} e^{-(\log(m)-\log(m_c))^2/2\sigma^2}/m & m < 1\,\mathrm{M}_\odot \\ m^{-2.3} & m > 1\,\mathrm{M}_\odot \end{cases} \tag{2.3}$$

with $m_c = 0{,}08\,\mathrm{M}_\odot$ and $\sigma = 0.69$. And it is normalised such that $\int_{0{,}1\,\mathrm{M}_\odot}^{100\,\mathrm{M}_\odot} m\frac{dn}{dm}dm = 1$. Mass and metals are ejected back into the inter stellar medium (ISM) via Type II and Type Ia SNe explosions and stellar loss, the former of which are determined using the parameterisations for stars of different masses and metallicities by Hurley et al. [44]. The masses of Fe and O ejected into the ISM can be converted to a metal mass:

$$M_Z = 2.09M_O + 1.06M_{Fe} \tag{2.4}$$

according to the solar abundances of metals [45]. Stars with masses between 8 and $40\,\mathrm{M}_\odot$ explode into Type II SNe depositing a total energy of 10^{51}ergs into the ISM. The following fitting functions [46] for the emitted and synthesized metal are employed:

$$M_{Fe} = 0.375e^{-17.94/m}M_\odot \tag{2.5}$$

$$M_O = 27.66e^{-51.81/m}M_\odot \tag{2.6}$$

where m is the stellar mass (in units of $M_\odot$). The number of Type Ia SNe for each timestep is adopted using the delay time distribution by Maoz et al. [47]. They leave nothing left and produce:

$$M_{Fe} = 0{,}63\,\mathrm{M}_\odot \qquad M_O = 0{,}14\,\mathrm{M}_\odot \tag{2.7}$$

according to the carbon deflagration model W7 by Iwamoto et al. [48].
Low mass stars below $8\,\mathrm{M}_\odot$ evolve and leave behind white dwarves emitting a great part of their mass to the ISM. In the simulations we are accounting for this with the empirical initial-final mass relation for white dwarfs by Kalirai et al. [49]:

$$w_m = (0.394 + 0.109m)\,M_\odot \tag{2.8}$$

for initial masses m between 1 and $8\,\mathrm{M}_\odot$. For stars between 8 and $m_{BH} = 40\,\mathrm{M}_\odot$ it is further assumed that they only return a $w_m = 1{,}4\,\mathrm{M}_\odot$ remnant. Stars above that

collapse into a black hole $w_m = m$. The integrated mass fraction of each generation of stars that is put back into the ISM over a Hubble time is then:

$$R = \int_{1\,\mathrm{M}_\odot}^{40\,\mathrm{M}_\odot} (m - w_m)\,\frac{dn}{dm} dm = 0.41 \tag{2.9}$$

Chapter 3

Analysis Code

In the following I will introduce the analysis code, which I made publicly available online[1], established for analysing the kinematics and morphology of the galaxies featured in the simulations.

3.1 Basic Considerations

Hydrodynamical simulations give results that are of a very different nature than observational data. SPH simulations give full phase space information for each particle and also provide lots of other interesting information like mass, density, and chemical composition. This is why the analysis code can make use of all of this directly instead of reconstructing it from observational data, which can be prone to large uncertainties.
When analysing things like galaxy rotation curves and radial DM density profiles it is by definition essential to transform the coordinates to a coordinate system that is centred around the galactic centre and rotated in such a way that the galactic disk is inside a coordinate plane. Also it is important to rid the velocity data of the centre of mass velocity.
In my code this is conducted in the following ways which are slightly different for isolated galaxy simulations and galactic scale zoom-in simulations:
The data which is saved in hdf5-files is first read with either PGFREADER [50] or YT [51]. Then, for the isolated case I first calculate the centre of mass of all particles with before specified particle types and then centre the coordinate system around the highest density gas particle within a sphere of 1 kpc around this centre of mass or if there are no gas particles in this sphere centre it right at the centre of mass. This method is a generalised version of the one used in the analysis of isolated galaxies by the *AGORA* collaboration [2], which only calculates the gas particles centre of mass in the first step. Next I subtract the centre of mass velocity from all the particles velocity vector. This calculation involves all particle types. For the rotation of the

[1] The analysis code can be downloaded from:
https://github.com/leonardromano/GalaxySimulationAnalysis

data in what I call the "disk frame", which has the galactic disk in the x-y plane I have implemented different options which can yield very different results for which the best has to be verified for each halo individually. All options agree on projecting the phase space coordinates on a right handed orthonormal system with the z-axis parallel to a mean angular momentum vector. One option calculates the density weighted mean angular momentum vector of all the gas particles. This is supposed to work well as the gas particles inside the disk which are mainly rotating inside this disk are having densities which are larger by orders of magnitude compared to the gas outside the disk. The other option calculates the non-weighted mean of the angular momentum of all particles in a specified list of particle types. This works especially well for disk and star particles as they are usually just rotating with the disk. The alignment to the disk frame is the most difficult and also most crucial part of the analysis, but unfortunately a general solution to this problem could not be found.
For the galactic scale zoom-in simulation first the position and radius of the halo have to be found. I implemented two different methods which are working equivalently well. The first method uses YT [51] to create a halo catalogue using the HOP halo finder [52] and then selects the most massive halo within a few Mpc of the central high resolution region. To sort out uninteresting halos the mass bounds and distance from the central region can be set. The second method allows to manually input the virial radius and position of the halo. This information can be for example be obtained using SPLASH [53]. Then all the data points that are outside the virial radius of the halo are dumped so that only the halo data remains. After this step the same methods as for the isolated case are used with the small difference that I added options to reduce the gas particles to only particles below a certain temperature and also reduce the gas and star particles to only the ones with $|z| \leq z_0$ after rotating to the disk frame to get cleaner statistics.

3.2 DM Velocity Distributions

DM velocity distributions are crucial for the analysis of observational DM data [54]. This is why it is of importance to study them not just using observational data, but also using simulations.
My analysis code uses the velocity data of the DM halo to extract normalised DM velocity- and speed-distributions and plot them as histograms.
The code splits the corresponding sector of the velocity spaces ($|v|$, v_ρ, v_φ, v_x, v_y, v_z) in bins with a fixed size and then counts the number of particles corresponding to each bin. It is possible to add fit-parameters for generalised Maxwellian and Gaussian distributions to plot them with the data, and it is also possible to plot the MW Standard Halo Model(SHM) speed distribution [54] or for the isolated case the

IC speed distribution [1] with the speed data. Additionally the result can also be saved as a png- and txt-file.

3.3 Rotation Curves

Galactic rotation curves contain lots of information about the morphology and kinematics of Galaxies. The shape of a rotation curve is also an important criterion to see if a galaxy is milky-way-like or not [55].
My analysis code offers lots of different options for creating rotation curves.
The first option plots the Keplerian rotation curve as predicted by the mass distribution of the halo and also the contributions of the single components. To do this the cylindrical radial domain is split into bins for each of which the rotational velocity is calculated using the well-known relation:

$$v_\varphi = \sqrt{\frac{GM(<r)}{r}} \tag{3.1}$$

Where G is the gravitational constant, r is the cylindrical radius and $M(<r)$ is the mass enclosed by the cylinder of radius r. The results are then plotted in one picture to compare the contributions of the single constituents. It is worth to note that this is not the actual rotation curve and can differ greatly from the one obtained from phase space data.
The second option makes the plot directly from the particles phase space data. The cylindrical radial domain is again split into bins and for each radial bin the mean rotational velocity is calculated separately for each particle type from a list of particle types. It is possible to calculate the mass weighted mean instead.[2] Further options include plotting data points as for example obtained from observational data, plotting the Keplerian rotation curve predicted by a NFW profile and also plotting the Keplerian rotation curve as predicted by the mass distribution in the same plot. The image and distribution data can be saved as png- and txt-files.

3.4 DM Density Profiles

To better understand the nature of DM a understanding of how DM is distributed in galaxies is crucial.
My code uses the position and mass data of the DM particles and calculates the DM radial density profile in a double logarithmic scale. To do this the logarithmic radial domain is split into bins and then for each bin the density is calculated using the following formula:

$$\rho_n = \frac{M\left(r_n < r < r_{n+1}\right)}{\frac{4\pi}{3}\left(r_{n+1}^3 - r_n^3\right)} \tag{3.2}$$

where r_n is the radial lower bound of the n-th bin and M ($r_n < r < r_{n+1}$) is the total mass of DM particles in the n-th bin. This method makes uses of the assumption that the DM density distribution is spherically symmetric.
The density profile is then plotted as a histogram and can be saved as a png- and txt-file. Optionally one can also include an NFW fit, place a horizontal bar at the value of the local DM density, include a horizontal bar at the value of the critical overdensity and include fitting functions in general.

3.5 Column Density Plots

To verify if the code really rotates the galaxy in the disk frame, centres it around the galactic centre and also to see if the disk can even be resolved it is useful to look at column density projection plots.
For isolated galaxies you can usually check this just by using available software like SPLASH [53], but for the zoom-in simulations this can be really complicated, which is why my analysis code includes the option to make these plots from the gas position, density and SPH smoothing length data (see 3.5.1).
The code takes the spatial bounds of the plot and the bin number as parameter and then calculates the density that falls in each three dimensional bin, using the following smoothing kernel:

$$W(r,h) = \begin{cases} \frac{1-6\left(\frac{r}{h}\right)^2+6\left(\frac{r}{h}\right)^3}{\pi h^3} & \text{if } 0 \leq r \leq 0.5h \\ \frac{2\left(1-\left(\frac{r}{h}\right)\right)^3}{\pi h^3} & \text{if } 0.5h < r \leq h \\ 0 & \text{if } h < r \end{cases} \tag{3.3}$$

where r is the distance from the centre of the gas particle and h is the smoothing length. The three dimensional density information is than summed up in the lines of sight yielding the two dimensional column density array. The column density array is then plotted as a two dimensional histogram in the log scale. The images can also be saved as png-files.

3.5.1 Understanding the SPH Smoothing Length

To better understand why the column density plots can or cannot resolve the galactic disk, I implemented the option to plot SPH smoothing length against the gas particles density. As a rule of thumb one can say that the disk can be resolved if the minimum smoothing length – which can be associated with the highest density gas particles and therefore the centre of the disk – has about the same order of magnitude as the width of the filaments in the disk. If the smoothing length is too large the high density particles just get smeared across the whole galaxy which leads to almost

ball-like disks (compare figure 14). If it were shorter than the distance between the particles it would no longer be smooth.

3.6 Local Value Calculations

Observational results give very clear values for the local DM density and the local rotational velocity [3]. This is why comparison of local values – values that are measured at the solar radius $R_\odot = (8{,}122 \pm 0{,}031)\,\mathrm{kpc}$ [56] from the galactic centre – taken from the simulation data with the observational data can be useful to see how well a MW simulation is reproducing the MW.
My code calculates the average rotational velocity and DM mass density around for different bin sizes around $R_\odot$ and from that then calculates the weighted averages over all bin sizes. The rotational velocity is calculated separately from the velocity data for each particle type. The results only include the statistical uncertainties from the calculates but do not assume the systematic uncertainties from the simulations. The results can then be returned as a txt-file.

Chapter 4

Results and Discussion

In this chapter I will present and discuss the results of my analysis. First I show the results for different snapshots from the isolated galaxy and zoom-in simulations. Then I present the local values I obtained and compare them to the latest observational results.

4.1 Isolated Galaxies

Here I present the results from the isolated galaxy simulation snapshots at $t \in \{1\,\mathrm{Gyr}, 5\,\mathrm{Gyr}, 10\,\mathrm{Gyr}\}$.

4.1.1 t = 1 Gyr

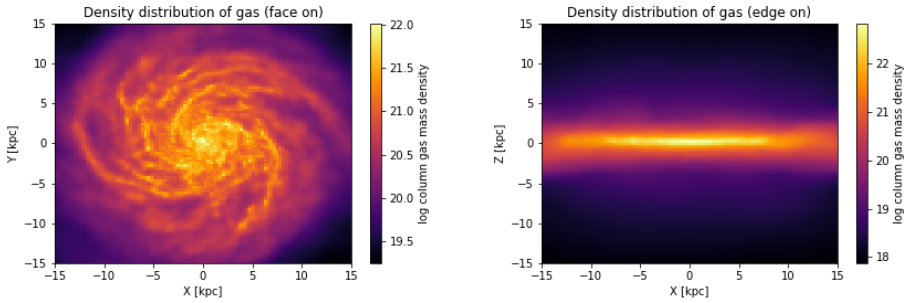

Figure 1: The $t = 1\,\mathrm{Gyr}$ snapshot of the isolated galaxy simulation. Shown are the gas column density plots in a $30\,\mathrm{kpc}$ box, face-on (left) and edge-on (right), produced with the code described in Section 3.5. As can be clearly seen the disk can be resolved.

At $t = 1\,\mathrm{Gyr}$ the galactic disk which is shown in figure 1 can be resolved. This is also in accordance with the smallest smoothing length, which is $h_{sml,min} \sim \mathcal{O}\,(10\,\mathrm{pc})$

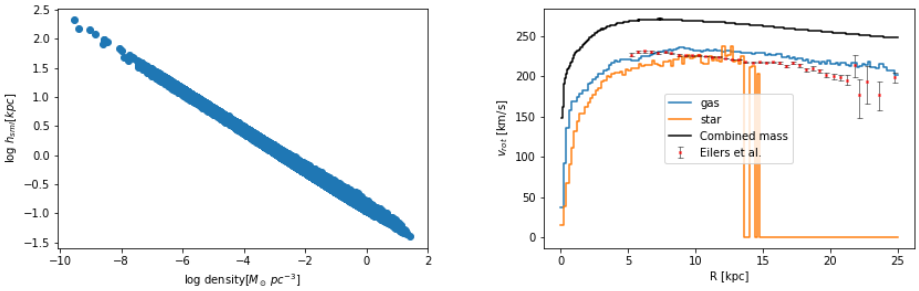

(a) (b)

Figure 2: The smoothing length vs. density plot (a) and the rotation curve (b) of the $t = 1\,\mathrm{Gyr}$ snapshot of the isolated disk.

as can be seen in figure 2a, which shows the smoothing length plotted double logarithmically against the gas density.
The total mass of the halo is $M_{tot} = 1{,}30 \times 10^{12}\mathrm{M}_\odot$ which is the combined mass of DM ($M_{200} = 1{,}25 \times 10^{12}\mathrm{M}_\odot$), gas ($M_{gas} = 7{,}25 \times 10^{9}\mathrm{M}_\odot$) and stellar mass ($M_\star = 4{,}00 \times 10^{10}\mathrm{M}_\odot$). Comparing this to the criteria for MW-like halos [55] – namely $5 \times 10^{11} < M_{200}[M_\odot] < 1 \times 10^{14}$ and $4.5 \times 10^{10} < M_\star[M_\odot] < 8.3 \times 10^{10}$ – this halo is not MW-like as there is too few stellar mass. However it is very close and the dynamics are very similar to those of the MW.
This can be seen, when looking at the gas and star rotation curves (figure 2b), which are in good accordance with the observational results, plotted alongside the data, over a broad domain. Only the steep rise in the inner region due to the stellar bulge [3] cannot be reproduced. Combining this with the fact that there is too few

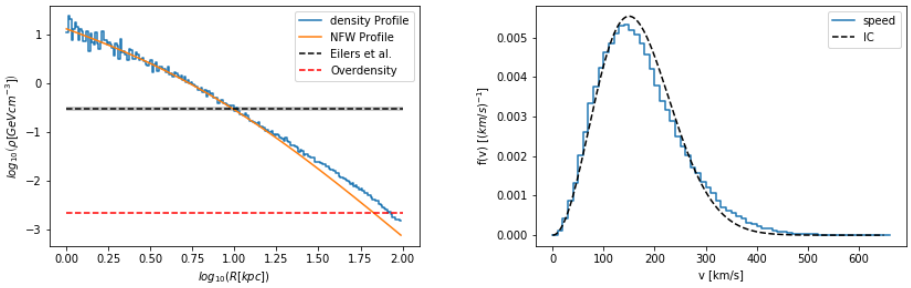

(a) (b)

Figure 3: The DM density profile (a) and the DM speed distribution (b) of the $t = 1\,\mathrm{Gyr}$ snapshot of the isolated disk.

stellar mass, I suggest to raise the amount of bulge mass in future simulations. Furthermore looking at the predicted rotation curve shown in black, it is puzzling why the actual rotational velocity is so much lower than the one predicted by the mass distribution.
The radial DM profile, shown in figure 3a can be fit very well with a NFW profile with
$r_s = (6{,}8 \pm 0{,}5)\,\mathrm{kpc}$ and $\rho_s = (0{,}63 \pm 0{,}08)\,\mathrm{GeV\,cm^{-3}}$. This profile is quite different from the initial profile as described in section 2.2.1. The NFW profile is cuspy, so if baryonic feedback were to solve the cusp-core problem for sufficiently strong feedback, in this simulation the feedback would be too weak. The obtained value for the local DM density, which is discussed in more detail in section 4.3 is also slightly higher than the observational value. For comparison the critical overdensity and the observed local DM density [3] are plotted as horizontal bars.
The DM speed distribution (figure 3b) is still very close to the initial conditions. This is no surprise as DM particles are collisionless so they should not vary much from the initial distribution.

4.1.2 t = 5 Gyr

The results at $t = 5\,\mathrm{Gyr}$ do not differ much from the results at $t = 1\,\mathrm{Gyr}$ as can be seen in figures 4 to 6b, which show the same plots for the different data. However there are some developments that I will point out here.
Due to star formation some of the gas has been transformed into stars changing the respective masses: $M_{gas} = 5{,}83 \times 10^9 \mathrm{M}_\odot$ and $M_\star = 4{,}14 \times 10^{10} \mathrm{M}_\odot$. However the stellar mass component is still not enough for the halo to be called MW-like

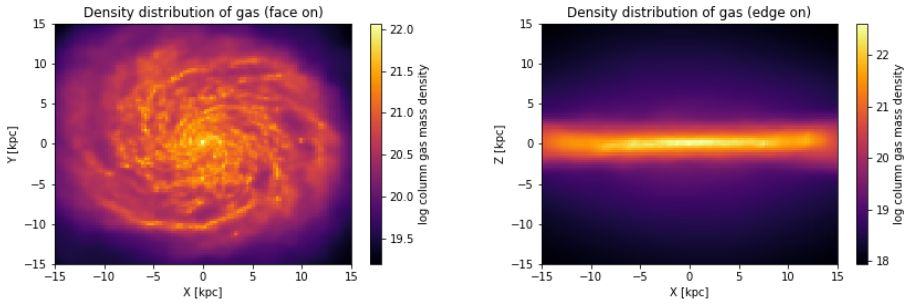

Figure 4: The $t = 5\,\mathrm{Gyr}$ snapshot of the isolated galaxy simulation.Shown are the gas column density plots in a 30 kpc box, face-on (left) and edge-on (right), produced with the code described in Section 3.5. As can be clearly seen the disk can be resolved.

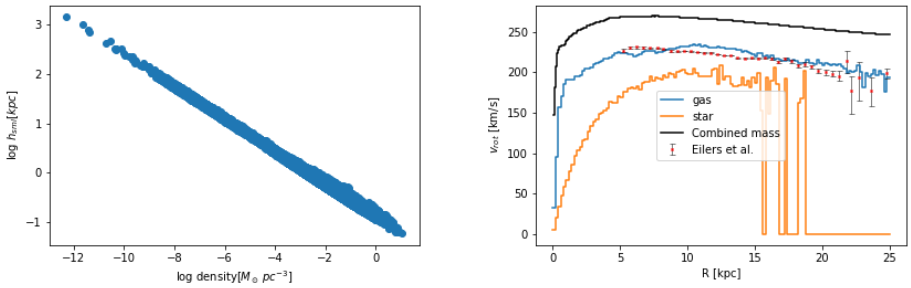

(a) (b)

Figure 5: The smoothing length vs. density plot (a) and the rotation curve (b) of the $t = 5\,\mathrm{Gyr}$ snapshot of the isolated disk.

according to the criteria mentioned above.
Also as can be seen in figure 5b the star particles rotation curve suddenly starts to fall to lower velocities, whereas the gas rotation curve hardly changes. This is a common problem in isolated galaxy simulations.
The DM density profile in figure 6a is still fit very well by a NFW profile. However it has become compactified with a higher scale density $\rho_s = (0{,}79 \pm 0{,}09)\,\mathrm{GeV\,cm^{-3}}$ and a smaller scale radius $r_s = (5{,}9 \pm 0{,}5)\,\mathrm{kpc}$. So the DM seems to effectively clump over time. Stronger baryonic feedback might counter this effect. The local density is again higher than the observational value.
The DM speed distribution in 6b is tilting slightly towards slower velocities. However this might just be due to statistical fluctuations.

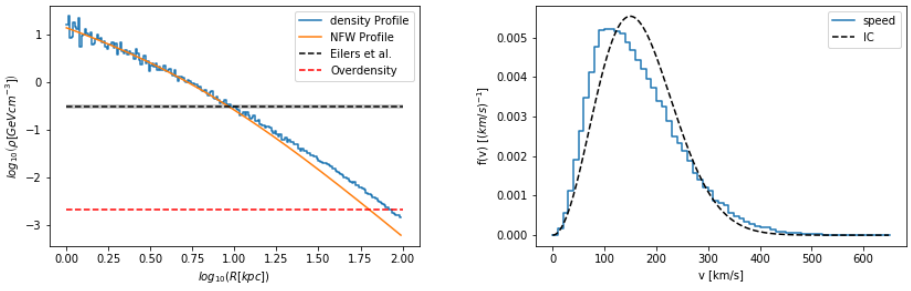

(a) (b)

Figure 6: The DM density profile (a) and the DM speed distribution (b) of the $t = 5\,\mathrm{Gyr}$ snapshot of the isolated disk.

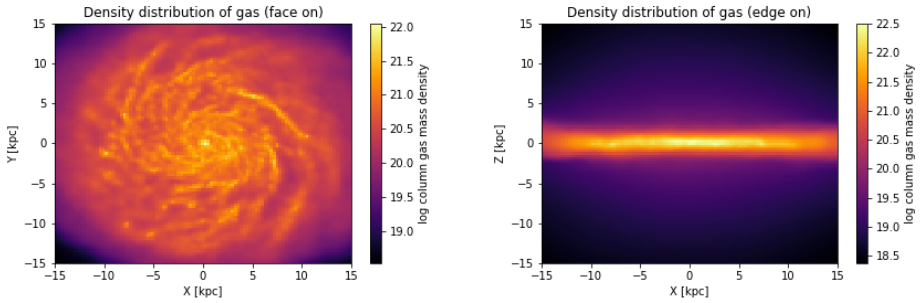

Figure 7: The $t = 10\,\mathrm{Gyr}$ snapshot of the isolated galaxy simulation. Shown are the gas column density plots in a 30 kpc box, face-on (left) and edge-on (right), produced with the code described in Section 3.5. As can be clearly seen the disk can be resolved.

4.1.3 t = 10 Gyr

As for the $t = 5\,\mathrm{Gyr}$ snapshot, I will shortly discuss the development that occurred between the $t = 10\,\mathrm{Gyr}$ snapshot and the previous ones, as depicted in figures 7 to 9b. The stellar and gas mass changed to $M_\star = 4{,}21 \times 10^{10}\mathrm{M}_\odot$ and $M_{gas} = 5{,}14 \times 10^{9}\mathrm{M}_\odot$ respectively. This change was very small and still did not raise the stellar mass in the preferred range.
Looking at the rotation curve (figure 8b) the trend a declining star rotation curve continues. Also now the gas rotation curve starts to decline at $r \sim 17\,\mathrm{kpc}$.
The trend of the compactifying DM density profile continues as well as can be seen

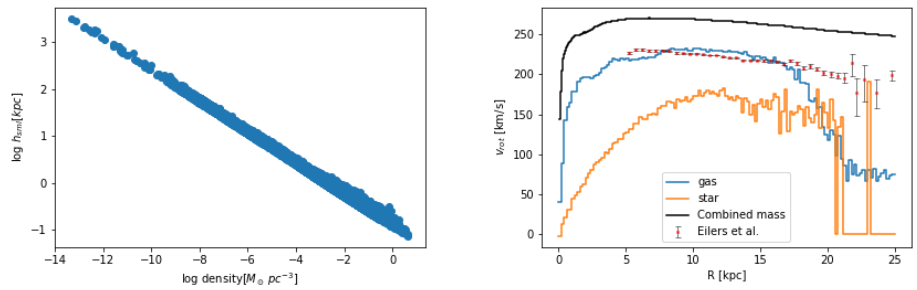

(a) (b)

Figure 8: The smoothing length vs. density plot (a) and the rotation curve (b) of the $t = 10\,\mathrm{Gyr}$ snapshot of the isolated disk.

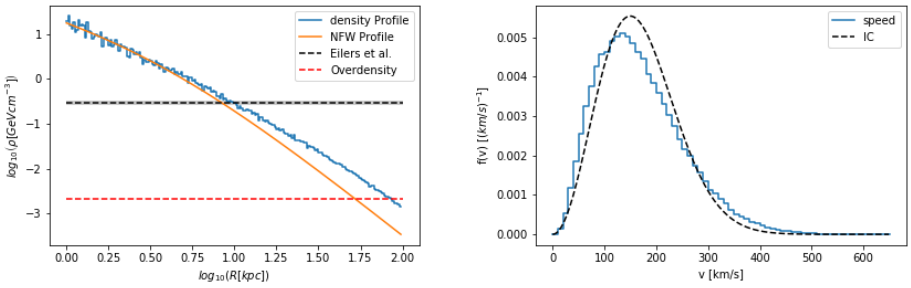

(a) (b)

Figure 9: The DM density profile (a) and the DM speed distribution (b) of the $t = 10\,\mathrm{Gyr}$ snapshot of the isolated disk.

in figure 9a. The scale radius is now shrunk to $r_s = (3{,}43 \pm 0{,}20)\,\mathrm{kpc}$ and the scale density is rising up to $\rho_s = (2{,}15 \pm 0{,}21)\,\mathrm{GeV\,cm^{-3}}$. This means that the DM clumps at an accelerated rate, which is characteristic for gravitational attraction. Again the local density is higher than the observational value.
As can be seen in figure 9b the DM velocity distribution is again shifting back towards the initial distribution.

4.2 Zoom-In Simulations

In this section I am presenting the results I got from the analysis of the galactic zoom-in simulation in a similar manner to the isolated disk simulation. First I will describe the snapshots at redshifts $z = 0.6$ and $z = 0.0$ for the level 10 simulation. Then describe the snapshot at redshift $z = 0.6$ for the level 11 simulation. Unfortunately a snapshot for level 11, $z = 0$ is not yet available. In all cases I am only analysing the main galaxy, which is found inside a sphere of radius 4,3 Mpc of the centre of the simulation.

4.2.1 Level 10 Simulation

4.2.1.1 z = 0.6

At $z = 0.6$ the disk which has a radius of $r_{Disk} \sim 10\,\mathrm{kpc}$ can not be resolved (figure 10). This can also be seen when looking at the smallest smoothing length in figure 11, which is of order $\mathcal{O}\,(1\,\mathrm{kpc})$, so clearly not able to resolve the disk.
The separate mass contributions are $M_{200} = 50{,}20 \times 10^{10}\mathrm{M}_\odot$, $M_\star = 3{,}32 \times 10^{10}\mathrm{M}_\odot$ and $M_{gas} = 4{,}98 \times 10^{10}\mathrm{M}_\odot$, which implies that this halo is not MW-like. It is also worth noting, that the gas mass is that high due to hot gas surrounding the

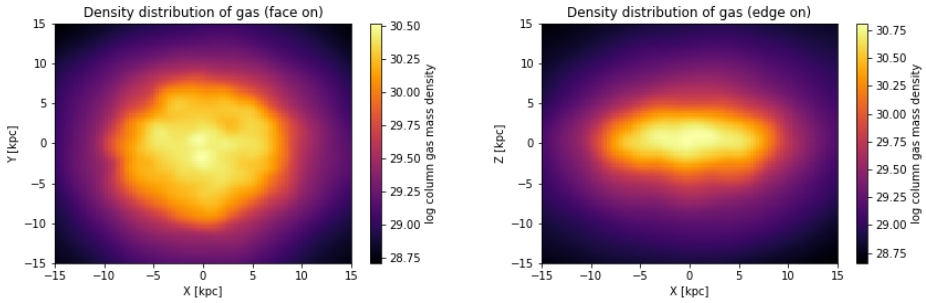

Figure 10: The main galaxy in the $z = 0.6$ snapshot of the level 10 zoom-in simulation. Shown are the gas column density plots in a 30 kpc box, face-on (left) and edge-on (right), produced with the code described in Section 3.5. As can be clearly seen the disk cannot be resolved.

galactic disk. If you just take the cold gas in the disk gas fractions in the order of $f_{gas} \sim \mathcal{O}(0.1)$ can be reproduced.
The rotation curve shown in figure 12 of this galaxy is much shallower than that of the Milky Way. Even the rotation curve which is predicted by the mass distribution is well below the observational values. However most notably when restricting the data only to the cold disk the gas rotation curve climbs above the mass distribution rotation curve and at one point almost reaches the observational values.
The radial DM density profile of this halo is shown in figure 13a. It is cuspy profile which can be fit quite well with a NFW profile with scale radius $r_s = (17{,}6 \pm 1{,}3)$ kpc and scale density $\rho_s = (0{,}062 \pm 0{,}007)\,\mathrm{GeV\,cm^{-3}}$. Again if baryonic feedback were

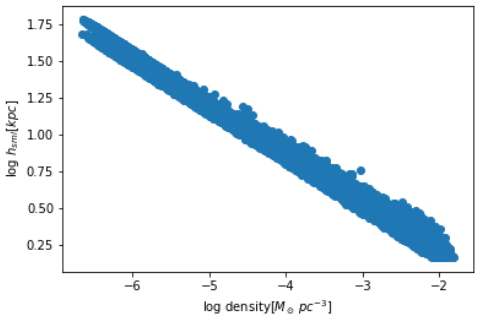

Figure 11: The SPH smoothing length vs. gas density plot for the $z = 0.6$ snapshot of the level 10 zoom-in simulation.

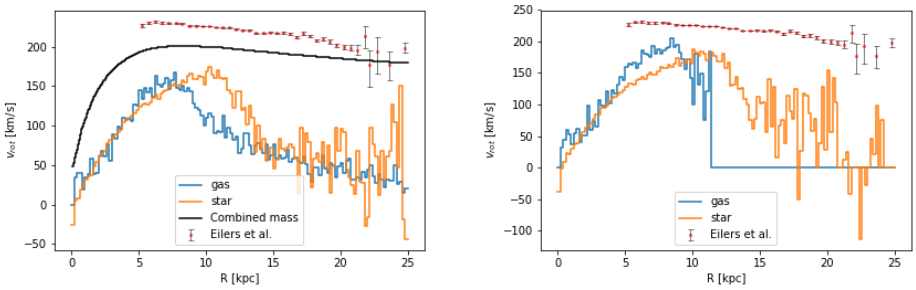

Figure 12: The rotation curve of the $z = 0.6$ snapshot of the level 10 zoom-in simulation. On the right the same results are shown after reducing the particles to those lying in the disk with $|z| < 1\,\mathrm{kpc}$ and gas particles with $log(T[K]) < 4$.

able to create cored profiles then the baryonic feedback in this simulation is just too weak, as the initial conditions with quiescent merger history were chosen. For the local DM density a value which is slightly lower than the observed value could be obtained. This is also consistent with the overall lower densities in this halo.
Figure 13b depicts the DM speed distribution which is slightly shifted towards slower speeds compared to the Milky-Way-SHM-distribution with a maximal rotational velocity $v_c = 220\,\mathrm{km\,s^{-1}}$. This is also consistent with the smaller mass content of the halo and the overall lower rotational velocities.

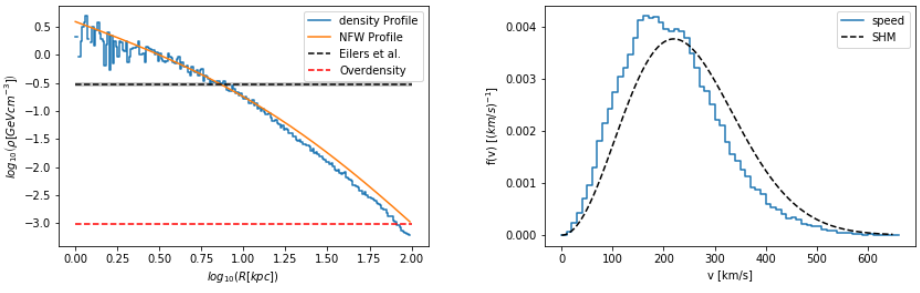

(a) (b)

Figure 13: The DM density profile (a) and the DM speed distribution (b) of the $z = 0.6$ snapshot of level 10 zoom-in simulation.

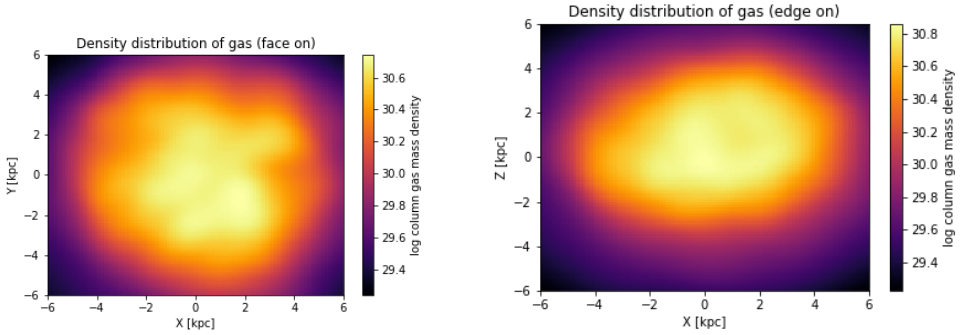

Figure 14: The main galaxy in the $z = 0.0$ snapshot of the level 10 zoom-in simulation. Shown are the gas column density plots in a 12 kpc box, face-on (left) and edge-on (right), produced with the code described in Section 3.5. As can be clearly seen the disk cannot be resolved.

4.2.1.2 z = 0.0

The radius of the disk which is shown in figure 14 at $z = 0.0$ is $r_{Disk} \sim 5\,\text{kpc}$. The disk can not be resolved for the same reason as for $z = 0.6$, which can be seen from figure 15. Also because of the small radius, the density weight angular momentum of gas which I used for the other snapshots is not very reliable, so instead I used the angular momentum of only the star particles.
The halo mass of the main galaxy $M_{200} = 73{,}51 \times 10^{10}\text{M}_\odot$, the stellar mass $M_\star = 3{,}90 \times 10^{10}\text{M}_\odot$ and the gas mass $M_{gas} = 8{,}57 \times 10^{10}\text{M}_\odot$ are pointing towards a not MW-like halo. However again reducing the data to only the cold disk gives a

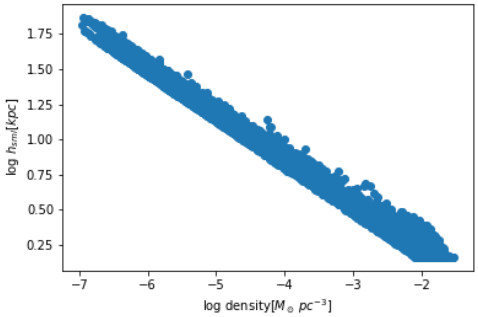

Figure 15: The SPH smoothing length vs. gas density plot for the $z = 0.0$ snapshot of the level 10 zoom-in simulation.

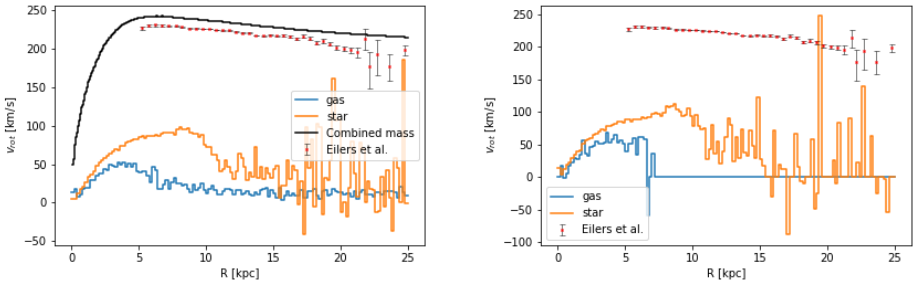

Figure 16: The rotation curve of the $z = 0.0$ snapshot of the level 10 zoom-in simulation. On the right the same results are shown after reducing the particles to those lying in the disk with $|z| < 1\,\text{kpc}$ and gas particles with $log(T[K]) < 4$.

reasonable gas fraction.
Figure 16 shows the rotation curve of the galaxy. For both gas and stars it is very shallow, even though the rotation curve predicted by the mass distribution would give slightly higher values than the observational results. Reducing the data to the cold disk does not change much.
The radial DM density profile shown in figure 17a can be fit arguably well by a NFW profile with scale radius $r_s = (20{,}7 \pm 1{,}4)\,\text{kpc}$ and scale density
$\rho_s = (0{,}080 \pm 0{,}007)\,\text{GeV}\,\text{cm}^{-3}$. The local density for this halo is higher than the observed value.
The speed distribution of this DM halo, shown in figure 17b, is very much shifted towards slower speeds compared to the SHM distribution. The maximum is located

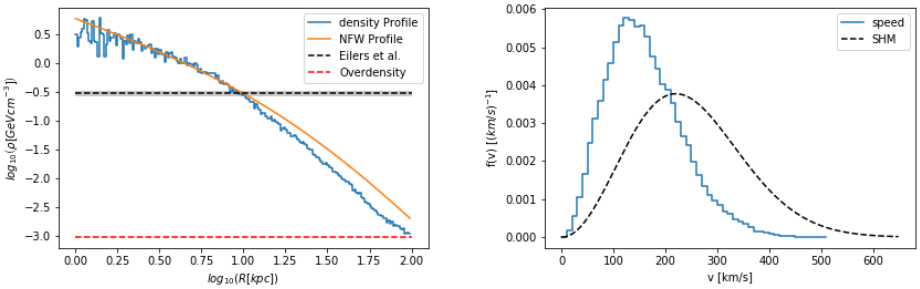

(a) (b)

Figure 17: The DM density profile (a) and the DM speed distribution (b) of the $z = 0.0$ snapshot of level 10 zoom-in simulation.

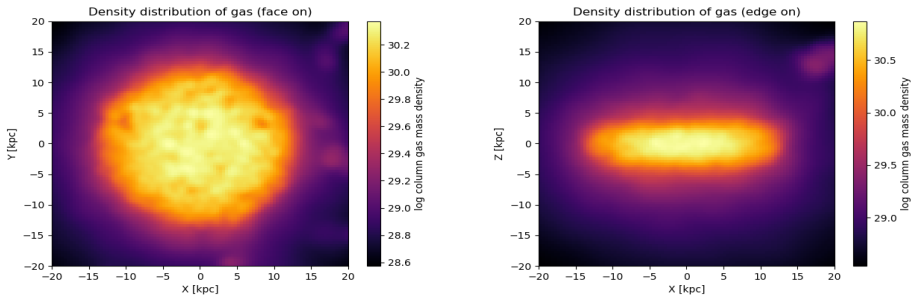

Figure 18: The main galaxy in the $z = 0.6$ snapshot of the level 11 zoom-in simulation. Shown are the gas column density plots in a 40 kpc box, face-on (left) and edge-on (right), produced with the code described in Section 3.5. As can be clearly seen the disk cannot be resolved.

somewhere around $v = 120\,\mathrm{kms}^{-1}$. Considering that this is supposed to be the same halo as for $z = 0.6$ at a later point this might be consistent with the gas and star speed also dropping significantly. Still it is hard to believe that the two galaxies are the same at different points in time considering how different their dynamics and morphology are. It is worth noting though that this will still likely be the case as in both cases the galaxies contain the greater part of the star particles.

4.2.2 Level 11 Simulation

The main galaxy in the level 11 simulation shown in figure 18 has a disk radius of $r_{Disk} \sim 15\,\mathrm{kpc}$, with a disk that cannot be resolved. Looking at the smallest

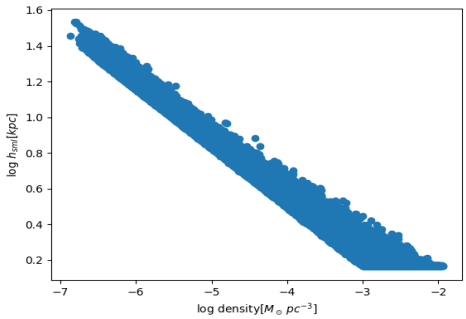

Figure 19: The SPH smoothing length vs. gas density plot for the $z = 0.6$ snapshot of the level 11 zoom-in simulation.

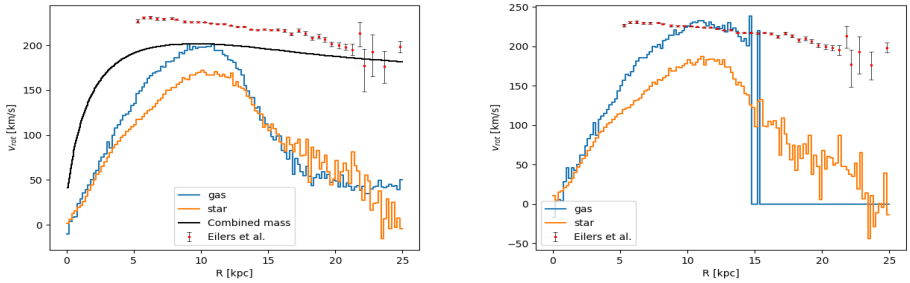

Figure 20: The rotation curve of the $z = 0.6$ snapshot of the level 11 zoom-in simulation. On the right the same results are shown after reducing the particles to those lying in the disk with $|z| < 1\,\mathrm{kpc}$ and gas particles with $log(T[K]) < 4$.

smoothing length (figure 19) this can also be verified.
The individual mass contributions come from the DM halo $M_{200} = 49{,}99 \times 10^{10} \mathrm{M}_{\odot}$, the gas $M_{gas} = 4{,}61 \times 10^{10} \mathrm{M}_{\odot}$ and the stellar disk $M_{\star} = 3{,}53 \times 10^{10} \mathrm{M}_{\odot}$, which again imply a not MW-like halo. Again a reasonable gas fraction can be obtained after reducing the data to the cold disk.
The rotation curve shown in figure 20 is slightly shallower than the MW one. When reducing the data to the cold disk, like for level 10 the gas rotation curves climbs above the mass distribution rotation curve.
The radial DM density profile of the main galaxy is shown in figure 21a. It has a 2 kpc core at slightly more than $\rho_{core} = 1\,\mathrm{GeV\,cm^{-3}}$. It is not very well fit by a NFW

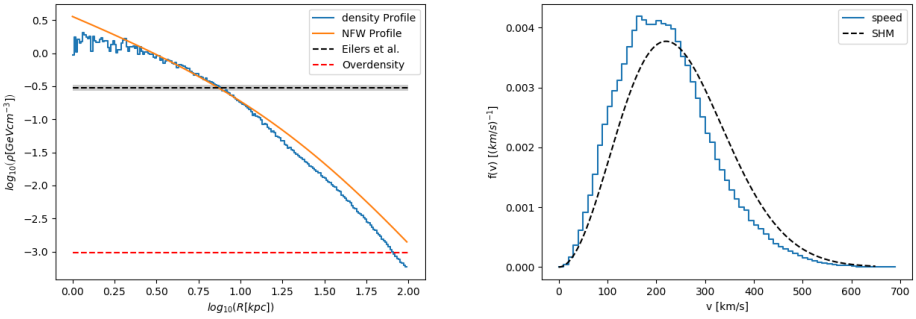

(a) (b)

Figure 21: The DM density profile (a) and the DM speed distribution (b) of the $z = 0.6$ snapshot of level 11 zoom-in simulation.

profile, but the non-cored part gave a scale radius $r_s = (22{,}6 \pm 0{,}9)\,\mathrm{kpc}$ and scale density $\rho_s = (0{,}0432 \pm 0{,}0023)\,\mathrm{GeV\,cm^{-3}}$ NFW profile, which is plotted alongside the data. This could be a successfully reproduced cored profile generated by baryonic feedback in a ΛCDM simulation. Moreover, the value for the local DM density is very close to the observed one.
The DM speed distribution shown in figure 21b is slightly shifted towards slower velocities compared to the SHM. Nevertheless this galaxy is much closer to the MW than in the level 10 simulation, suggesting that increasing the resolution – possibly even to a point where the disk can be resolved – might actually reproduce MW-like galaxies with cored profiles.

4.3 Local DM Mass Density and Rotational Velocity

In this section I am comparing the local values for DM density $\rho_\odot$ and rotational velocity $V_\odot$ with the observational latest observationalt results by Eilers et al. [3]. The results are shown in table 4.1. Note that for the level 10, $z = 0.0$ snapshot there is no $V_\odot$ value for the gas particles as the gas disk is not extended up to $R_\odot$.
The values for the local DM density are all within a factor of 1.5 of the observed value. The snapshot that reproduces it the best is the level 11 zoom-in simulation at $z = 0.6$. This snapshot seems to model the properties of the DM halo the best so this is no surprise.
The local rotational velocity can only be reproduced with all particle types in the $t = 1\,\mathrm{Gyr}$ snapshot of the isolated disk. For the other snapshots the value can vary up to an order of magnitude. However for all snapshots of the isolated disk the value for the gas is very close to the literature value. From all the zoom-in snapshots the level 11 simulation reproduces the rotational velocity the best, giving hope that maybe higher resolution can resolve this problem.

	$\rho_\odot[GeV\,cm^{-3}]$	$V_\odot[km\,s^{-1}]$ (gas)	$V_\odot[km\,s^{-1}]$ (stars)
Isolated, $t = 1\,\mathrm{Gyr}$	$0{,}431 \pm 0{,}003$	$232{,}54 \pm 0{,}06$ (gas)	$217{,}2 \pm 0{,}4$ (stars) $225{,}38 \pm 0{,}11$ (disk)
Isolated, $t = 5\,\mathrm{Gyr}$	$0{,}401 \pm 0{,}007$	$226{,}12 \pm 0{,}09$ (gas)	$193{,}5 \pm 0{,}4$ (stars) $207{,}91 \pm 0{,}18$ (disk)
Isolated, $t = 10\,\mathrm{Gyr}$	$0{,}394 \pm 0{,}006$	$230{,}16 \pm 0{,}13$ (gas)	$163{,}9 \pm 0{,}4$ (stars) $191{,}89 \pm 0{,}24$ (disk)
Level 10, $z = 0.6$	$0{,}241 \pm 0{,}003$	$148{,}2 \pm 1{,}0$ (gas) $183{,}1 \pm 0{,}7$ (cold disk)	$154{,}2 \pm 0{,}5$ (stars) $157{,}4 \pm 0{,}5$ (disk)
Level 10, $z = 0.0$	$0{,}411 \pm 0{,}005$	$24{,}5 \pm 0{,}8$ (gas)	$96{,}4 \pm 0{,}5$ (stars) $101{,}6 \pm 0{,}5$ (disk)
Level 11, $z = 0.6$	$0{,}2732 \pm 0{,}0013$	$186{,}31 \pm 0{,}27$ (gas) $203{,}7 \pm 0{,}3$ (cold disk)	$155{,}57 \pm 0{,}18$ (stars) $159{,}61 \pm 0{,}24$(disk)
Eilers et al.	$0{,}30 \pm 0{,}03$	$229{,}0 \pm 0{,}2$	

Table 4.1: The local DM density and the local rotational velocity from the different snaps are listed. For the zoom- in snapshots the keywords "disk" and "cold" mean, that only particles in the galactic disk or particles with temperatures below $T = 10^4\mathrm{K}$ have been used for the calculation.

Chapter 5

Conclusion and Outlook

In this work I have shown that a MW-like galaxy can be reproduced using SPH numerical simulations in the case of an isolated disk. This was realized by using the simulation code GADGET-3 and the initial conditions created with the MAKEDISK code written by Volker Springel [34, 35]. I also suggest to increase the amount of bulge mass in future simulations to better reproduce the MW rotation curve. I was also able to show that for the case of weak baryonic feed back cored DM profiles could not be reproduced for the isolated disk and instead DM continues to clump at accelerating speed.
By analysing the main galaxies in galactic scale zoom-in simulations I found that neither level 10 nor level 11 provide enough resolution to resolve the disk. MW-like halos were not able to be reproduced as the rotation curve was too shallow in all simulations. However for the higher resolution level 11 simulation a cored DM profile has been successfully reproduced with weak baryonic feedback. This is a critical result as it can help further understand the nature of the relationship between dark and baryonic matter and possibly give a hint towards the solution of some of the small scale problems mentioned in chapter 1.
The code I have written to analyse the snapshots created with GADGET-3 has also proven itself to be very robust and useful for extracting and presenting the simulation data, and I hope it can be further used and tuned to support future studies as well. The simulations run so far were only restricted to rather low resolution and only used weak baryonic feedback with small star formation rates, so it will be interesting to see how stronger baryonic feedback, higher resolution and higher star formation rates compete with other popular theories like SIDM [6], WIMPs [28, 29] and MOND [30, 31, 32] and what sort of results the implementation of them has to offer. It is however worth noting that higher resolution is combined with much higher computational costs setting clear limits for the resolution. This is why research of new methods for numerical calculations, implementation of artificial intelligence (AI) and better hardware will be needed to push the boundaries of numerical simulations and of our understanding of the fundamental principles of the universe. Also new observational results from large scale sky surveys like *ALMA* [57, 58] and the Large Synoptic Survey Telescope (LSST) [7] will help the cosmology community verify and improve their

results and maybe even provide a definite test for the ΛCDM paradigm.
Since these simulations are part of the *AGORA* project which aims to compare different simulation codes it will also be interesting to see what results are produced by the other participating codes which will be subject to future research.

List of Figures

Bibliography

[1] Kim, J.-h., Abel, T., Agertz, O., Bryan, G. L., Ceverino, D., Christensen, C.,..., Zolotov, A., & for the AGORA Collaboration. 2014, ApJS, 210, 14

[2] Kim, J., Abel, T., Teyssier, R., Butler, M.J., Ceverino, D., Choi, J., ..., Wise, J.H., & for the AGORA Collaboration. 2016, ApJ, 833, 202

[3] Eilers, A., Hogg, D.W., Rix, H., Ness & Ness, M. 2018, arXiv:1810.09466 [astro-ph.GA]

[4] Zwicky, F. 1937 ApJ, 86, 217

[5] Bahcall, N.A., Ostriker, J.P., Perlmutter, S., Steinhardt, P.J. 1999, Science 284 1481. astro-ph/9906463.

[6] Tulin, S. and Yu, H. 2018, Physics Reports, 730, pp.1-57.

[7] Bullock, J.S. and Boylan-Kolchin, M. 2017, Annu. Rev. Astron. Astrophys. 55:343–87.

[8] Dubinski, J., Carlberg,R.G. 1991, ApJ, 378, 496.

[9] Navarro, J.F., Frenk, C.S., White, S.D.M. 1996, ApJ, 462, 563. astro-ph/9508025.

[10] Navarro, J.F., Frenk, C.S., White, S.D.M. 1997, ApJ, 490, 493. astro-ph/9611107.

[11] Flores, R.A., Primack, J.R. 1994 ApJ. 427, L1. astro-ph/9402004.

[12] Moore, B. 1994 Nature 370, 629.

[13] Moore, B., Quinn, T.R., Governato, F., Stadel, J., Lake, G. 1999 Mon. Not. R. Astron. Soc. 310, 1147. astro-ph/9903164.

[14] Bullock, J.S., Kolatt, T.S., Sigad, Y., Somerville, R.S., Kravtsov, A.V., Klypin, A.A., Primack, J.R. & Dekel, A. 2001, Mon. Not. R. Astron. Soc. 321, 559. astro-ph/9908159.

[15] Oman, K.A., et al. 2015, Mon. Not. R. Astron. Soc. 452, 3650. arXiv:1504.01437.

[16] Kuzio de Naray, R., Martinez, G.D., Bullock, J.S., Kaplinghat, M. 2010 ApJ, 710, L161. arXiv:0912.3518.

[17] Kauffmann, G., White, S.D.M., Guiderdoni, B. 1993, Mon. Not. R. Astron. Soc. 264, 201.

[18] Moore, B., Ghigna, S., Governato, F., Lake, G., Quinn, T.R., Stadel, J., Tozzi, P. 1999 ApJ 524, L19. astro-ph/9907411.

[19] Klypin, A.A., Kravtsov, A.V., Valenzuela, O., Prada, F. 1999 ApJ 522, 82. astro-ph/9901240.

[20] Trujillo-Gomez, S., Klypin, A., Primack, J., Romanowsky, A.J. 2011 ApJ 742, 16. arXiv:1005.1289.

[21] Zavala, J., Jing, Y.P., Faltenbacher, A., Yepes, G., Hoffman, Y.,Gottlober, S., Catinella, B. 2009 ApJ 700, 1779. arXiv:0906.0585.

[22] Zwaan, M.A., Meyer, M.J., Stayeley-Smith, L. 2010, Mon. Not. R. Astron. Soc. 403, 1969. arXiv:0912.1754.

[23] Kim, S.Y., Peter, A.H.G., Hargis, J.R. 2018, Phys. Rev. Lett. 121, 211302. arXiv:1711.06267

[24] Boylan-Kolchin, M., Bullock, J.S., Kaplinghat, M. 2011 Mon. Not. R. Astron. Soc. 415, L40. arXiv:1103.0007.

[25] Boylan-Kolchin, M., Bullock, J.S., Kaplinghat, M. 2011 Mon. Not. R. Astron. Soc. 422, 1203. arXiv:1111.2048.

[26] Tollerud, E.J., Boylan-Kolchin, M., Bullock, J.S. 2014, Mon. Not. R. Astron. Soc. 440, 3511. arXiv:1403.6469.

[27] Garrison-Kimmel, S., Boylan-Kolchin, M., Bullock, J.S., Kirby, E.N. 2014 Mon. Not. R. Astron. Soc. 444, 222. arXiv:1404.5313.

[28] Goldberg, H. 1983, Phys. Rev. Lett. 50, 1419; 2009, Phys. Rev. Lett. 103, 099905 (erratum).

[29] Jungman, G., Kamionkowski, M. & Griest, K. 1996, Phys. Rep. 267, 195. hep-ph/9506380.

[30] Milgrom M. 2002, New Astron. Rev. 46:741–753

[31] Famaey B., McGaugh SS. 2012, Living Reviews in Relativity 15:10

[32] McGaugh, SS. 2015, Canadian Journal of Physics 93:250–259

[33] Farnes, J. 2018, A&A, 620, A92.

[34] Springel, V., Yoshida, N., & White, S. D. M. 2001, New Astronomy, 6, 79

[35] Springel, V. 2005, MNRAS, 364, 1105

[36] Springel, V., Wang, J., Vogelsberger, M., Ludlow, A., Jenkins, A., Helmi, A., ... & White, S. D. M. 2008, MNRAS, 391, 1685

[37] Hernquist, L. 1990, ApJ, 356, 359

[38] Hahn, O., & Abel, T. 2011, MNRAS, 415, 2101

[39] Planck Collaboration: Ade, P.A.R., Aghanim, N., Arnaud, M., Ashdown, M., Aumont, J., Baccigalupi, C. et. al. 2016, A&A, 594, A13

[40] Smith, B. D., Bryan, G. L., Glover, S. C. O., Goldbaum, N. J., Turk, M. J.; Regan, J., ... & Khochfar, S. 2017, MNRAS, 466, 2217S

[41] Ferland, G. J., Porter, R. L., van Hoof, P. A. M., Williams, R. J. R., Abel, N. P., Lykins, M. L., ... & Stancil, P. C. 2013, Revista Mexicana de Astronomia y Astrofisica, 49, 137

[42] Haardt, F., & Madau, P. 2012, ApJ, 746, 125

[43] Chabrier, G. 2003, ApJL, 586, L133

[44] Hurley, J. R., Pols, O. R., & Tout, C. A. 2000, MNRAS, 315, 543

[45] Asplund, M., Grevesse, N., Sauval, A. J., & Scott, P. 2009, ARAA, 47, 481

[46] Woosley, S. E., & Heger, A. 2007, Phys. Rep., 442, 269

[47] Maoz, D., Mannucci, F., & Brandt, T. D. 2012, MNRAS, 426, 3282

[48] Iwamoto, K., Brachwitz, F., Nomoto, K., Kishimoto, N., Umeda, H., Hix,W. R., & Thielemann, F.-K. 1999, ApJS, 125, 439

[49] Kalirai, J. S., Hansen, B. M. S., Kelson, D. D., Reitzel, D. B., Rich, R. M., & Richer, H. B. 2008, ApJ, 676, 594

[50] Thompson, R. 2014, ascl:1411.001

[51] Turk, M. J., Smith, B. D., Oishi, J. S., Skory, S., Skillman, S. W., Abel, T., & Norman, M. L. 2011, ApJS, 192, 9

[52] Eisenstein, D. J., & Hut, P. 1998, ApJ, 498, 137

[53] Price, 2007, Publ. Astron. Soc. Aust., 24, 159-173

[54] Bozorgnia, N. and Bertone, G. 2017, arXiv:1705.05853 [astro-ph.CO]

[55] Bozorgnia, N., Calore, F., Schaller, M., Lovell, M., Bertone, G., Frenk, C. S., ... & Theuns, T. 2016, JCAP 1605 (2016), no. 05 024, [arXiv:1601.04707].

[56] Gravity Collaboration, Abuter, R., Amorim, A., et al. 2018, A&A, 615, L15

[57] Hezaveh, Y.D. et al. 2016 Astrophys. J. 823, 37. arXiv:1601.01388.

[58] Inoue, K.T., Minezaki, T., Matsushita, S. & Chiba, M. 2016, Mon. Not. R. Astron. Soc. 457, 2936. arXiv:1510.00150.

Acknowledgements

Hereby I would like to thank the whole research group of Kentarō Nagamine for the awesome semester I have spent in Osaka. Special thanks go to

Ken for always challenging me with interesting research problems and being the best mentor one can imagine

Björn Garbrecht for being my supervisor at TUM

Kazunori for providing me with the snapshots of the zoom-in simulations and helping me with the code for the column density plot

Ikko for providing me with the snapshots of the isolated disk simulations

Abed for being the first person to ask about anything and for all the jokes

Kahmin and **Robin** for bringing the "fizz" into "office"

And lastly **all the people from F513**, who were the best office mates one could imagine.

And of course the rest, who make this group a place to be!

Erklärung der selbstständigen Anfertigung

Mit der Abgabe dieser Bachelorarbeit versichere ich, dass ich die vorliegende Arbeit selbstständig und ohne Benutzung anderer als der angegebenen Hilfsmittel angefertigt habe. Alle Stellen, die wörtlich oder sinngemäß aus Veröffentlichungen entnommen sind, wurden als solche kenntlich gemacht.

Diese Arbeit wurde in gleicher oder ähnlicher Form keiner anderen Prüfungsordnung vorgelegt.

Toyonaka, den 4. Februar 2019

_____

(Leonard Romano)